International Journal of Modern Physics B, Vol. 13, No. 18 (1999) 2405–2429

CRITICAL SCALING BEHAVIOR IN COUPLED MAGNETIC OSCILLATORS

SANG-YOON KIM*

Department of Physics, Kangwon National University Chunchon, Kangwon-Do 200-701, Korea

Received 10 February 1999
Revised 21 June 1999

We study the critical scaling behaviors of period doublings in N ($N = 2, 3, 4, \ldots$) coupled magnetic oscillators by varying the driving amplitude A and the coupling strength c. It is found that the critical scaling behaviors depend on the range of coupling. For the extreme long-range case of global coupling, the critical set (set of critical points) is composed of the zero-coupling critical point with $c = 0$ and an infinity of critical line segments in the $A - c$ plane, independently of N. Three kinds of critical scaling behaviors are found on the critical set. However, for any other nonglobal-coupling cases of shorter-range couplings, the structure of the critical set becomes different from that for the global-coupling case, because of a significant change in the stability diagram. We also note that the structure of the critical set and the critical scaling behaviors for both cases of the global and nonglobal couplings are the same as those in the abstract system of the coupled one-dimensional maps.

PACS number(s): 05.45.-a

1. Introduction

Coupled nonlinear oscillators have attracted considerable attention in recent years. They are used to model many physical, chemical and biological systems such as coupled p-n junctions,[1] Josephson-junction arrays,[2] the charge-density waves,[3] chemical-reaction systems,[4] and biological-oscillation systems.[5] Such coupled oscillators are known to exhibit diverse bifurcations, multistability, chaos, pattern formation and so on.

The coupled nonlinear oscillators studied here are coupled magnetic oscillators (MO's), consisting of N identical magnetic dipoles placed in a periodically oscillating magnetic field and coupled through some interaction mechanism. Each single MO is described by a normalized equation of motion,[6–9]

$$\ddot{x} = f(x, \dot{x}, t) = -\Gamma\dot{x} + A\cos 2\pi t \sin 2\pi x\,, \tag{1}$$

*Electronic address: sykim@cc.kangwon.ac.kr

where x is a normalized angle with range $\in [-\frac{1}{2}, \frac{1}{2})$, Γ is a normalized damping parameter and A is a normalized driving amplitude. This MO, albeit simple looking, exhibits a richness in its dynamical behaviors.[9] One of its interesting behaviors is a cascade of the "resurrections" of the stationary points. That is, as A is increased the stationary points restabilize after they lose their stability, destabilize again and so forth *ad infinitum*. For each case of the resurrections, an infinite sequence of period-doubling bifurcations follows and ends at its accumulation point A^*. When A exceeds A^*, a period-doubling transition to chaos occurs. Consequently, with increasing A an infinite series of period-doubling transitions to chaos occur successively, which will be referred to as "multiple period-doubling transitions to chaos".[10] This is in contrast to the one-dimensional (1D) map,[11] where only single period-doubling transition to chaos takes place. However, the critical scaling behaviors at each ith period-doubling transition point A_i^* $(i = 1, 2, 3, \ldots)$ are the same as those in the 1D map.

Recently, I and Kook found the three kinds of new critical behaviors of period doublings in the abstract system of coupled 1D maps.[12] This is an extension of the Feigenbaum's work[11] for the 1D map to the coupled maps. We also note that Feigenbaum criticality has been observed in a large of real systems. So, the fundamental question for the coupled case is: Do the new critical scaling behaviors found in the abstract system of the coupled 1D maps occur in a real coupled system? To discuss this question, we consider a real system of symmetrically coupled MO's and study the critical scaling behaviors for the case of various couplings. Note also that here we are interested only in the synchronous period doubling bifurcations of the synchronous orbits. Hence the fate of the system after its desynchronization through asynchronous bifurcations is not discussed here. It is thus found that both the structure of the critical set and the critical scaling behaviors in the coupled MO's are the same as those in the coupled 1D maps. Hence we believe that the critical scaling behaviors in the abstract system of the coupled 1D maps may be observed in a real system of coupled oscillators.

This paper is organized as follows. We first introduce N symmetrically coupled MO's in Sec. 2 and discuss stability, bifurcations and Lyapunov exponents of the synchronous orbits. We then investigate the critical scaling behaviors of period doublings in Secs. 3 and 4. As in the single MO,[9] the stationary points in the coupled MO's undergo multiple period-doubling transitions to chaos [e.g., see Figs. 2(a) and 5 for the stability diagrams, associated with the first and second period-doubling transitions to chaos, respectively]. For each period-doubling transition to chaos, the critical scaling behaviors vary depending on whether or not the coupling is global. We thus consider separately the global and nonglobal coupling cases in Secs. 3 and 4, respectively. For the extreme long-range case of global coupling, in which each MO is coupled to all the other ones with equal strength, the zero-coupling critical point with $c = 0$ and an infinity of critical line segments lying on the line $A = A_i^*$ constitute the same critical set in the $A-c$ plane, irrespectively of N. Three kinds of critical behaviors associated with the scaling of the coupling parameter c are found

on the critical set, while the critical scaling behaviors of the driving amplitude A are always the same as those in the uncoupled MO.[9] However, for any other nonglobal-coupling cases of shorter-range couplings, a significant change occurs in the stability diagram of the synchronous 2^n-periodic ($n = 1, 2, \ldots$) orbits born via period doublings in the $A - c$ plane. Consequently, the structure of the critical set becomes different from that for the global-coupling case. We also note that the structure of the critical set and the critical scaling behaviors for both cases of the global and nonglobal couplings are the same as those in the abstract system of the coupled 1D maps.[12] Finally, a summary is given in Sec. 5.

2. Stability, Bifurcations and Lyapunov Exponents

In this section we first introduce symmetrically coupled MO's and then discuss stability, bifurcations and Lyapunov exponents of synchronous orbits. Consider a system of N symmetrically coupled MO's with a periodic boundary condition,

$$\ddot{x}_m = f(x_m, \dot{x}_m, t) + g(x_m, x_{m+1}, \ldots, x_{m-1}), \qquad m = 1, 2, \ldots, N. \tag{2}$$

Here the periodic boundary condition imposes $x_m(t) = x_{m+N}(t)$ for all m, the function $f(x, \dot{x}, t)$ is given in Eq. (1) and $g(x_1, \ldots, x_N)$ is a coupling function, obeying the condition

$$g(x, \ldots, x) = 0 \qquad \text{for all } x. \tag{3}$$

The second-order differential equations (2) are reduced to a set of first-order differential equations,

$$\dot{x}_m = y_m, \tag{4a}$$

$$\dot{y}_m = f(x_m, y_m, t) + g(x_m, x_{m+1}, \ldots, x_{m-1}), \qquad m = 1, 2, \ldots, N. \tag{4b}$$

Note that these equations have a cyclic permutation symmetry, because they are invariant under the transformation σ,

$$(z_1, z_2, \ldots, z_N) \to (z_2, \ldots, z_N, z_1); \qquad z_m \equiv (x_m, y_m). \tag{5}$$

The set of all fixed points of the cyclic permutation σ forms a 2D synchronization plane, on which

$$x_1 = \cdots = x_N, \qquad y_1 = \cdots = y_N. \tag{6}$$

An orbit is called $a(n)$ (in-phase) synchronous orbit, if it lies on the synchronization plane, i.e., it satisfies

$$x_1(t) = \cdots = x_N(t) \equiv x^*(t), \qquad y_1(t) = \cdots = y_N(t) \equiv y^*(t). \tag{7}$$

Otherwise it is called an (out-of-phase) asynchronous orbit. Here we study only synchronous orbits. They can be easily found from the uncoupled MO (1), because

the coupling function g satisfies the condition (3). Note also that for these synchronous orbits with the cyclic permutation symmetry σ, the equations (4b) have two additional symmetries S_1 and S_2, because the transformations

$$S_1 : x_m \to -x_m\,, \qquad y_m \to -y_m\,, \qquad t \to t\,, \tag{8}$$

$$S_2 : x_m \to x_m \pm \frac{1}{2}\,, \qquad y_m \to y_m\,, \qquad t \to t \pm \frac{1}{2}\,, \tag{9}$$

leave Eq. (4b) invariant. The transformation S_1 is the (space) inversion, while the transformation S_2 is a shift in x_m and t. Hereafter we will call S_1 and S_2 the inversion and shift symmetries, respectively. If a synchronous orbit is invariant under S_i $(i = 1, 2)$, it is called an S_i-symmetric orbit. Otherwise, it is called an S_i-asymmetric orbit and has its "conjugate" orbit $S_i z(t)$.

We now discuss the couplings between the MO's. Consider an element, say the mth element, in the N coupled MO's. Then the $(m \pm \delta)$th elements are called the δth neighbors of the mth element. Here we consider the case where the coupling extends to the Kth $[1 \le K \le \frac{N}{2}(\frac{N-1}{2})$ for even (odd) $N]$ neighbor(s) with equal strength. Hereafter we will call the number K the range of the coupling interaction.

A general form of coupling for odd N $(N \ge 3)$ is given by

$$\begin{aligned} g(x_1, \ldots, x_N) &= \frac{c}{2K+1} \sum_{l=-K}^{K} [u(x_{1+l}) - u(x_1)] \\ &= c \left[\frac{1}{2K+1} \sum_{l=-K}^{K} u(x_{1+l}) - u(x_1) \right], \quad K = 1, \ldots, \frac{N-1}{2}\,, \end{aligned} \tag{10}$$

where c is a coupling parameter and u is a function of one variable. Note that the coupling extends to the Kth neighbors with equal coupling strength and the function g satisfies the condition (3). The extreme long-range interaction for $K = \frac{N-1}{2}$ is called a global coupling, for which the coupling function g becomes

$$\begin{aligned} g(x_1, \ldots, x_N) &= \frac{c}{N} \sum_{m=1}^{N} [u(x_m) - u(x_1)] \\ &= c \left[\frac{1}{N} \sum_{m=1}^{N} u(x_m) - u(x_1) \right]. \end{aligned} \tag{11}$$

This is a kind of mean-field coupling, in which each MO is coupled to all the other ones with equal coupling strength. All the other couplings with $K < (N-1)/2$ (e.g., nearest-neighbor coupling with $K = 1$) will be referred to as nonglobal couplings. The $K = 1$ case for $N = 3$ corresponds to both the global coupling and the nearest-neighbor coupling.

For even N $(N \ge 2)$, the form of coupling of Eq. (10) holds for the cases of nonglobal couplings with $K = 1, \ldots, (N-2)/2$ $(N \ge 4)$. The global coupling for $K = N/2$ $(N \ge 2)$ also has the form of Eq. (11), but it cannot have the form of

Eq. (10), because there exists only one farthest neighbor for $K = N/2$, unlike the case of odd N. The $K = 1$ case for $N = 2$ also corresponds to the nearest-neighbor coupling as well as to the global coupling, like the $N = 3$ case.

From now on, we discuss stability and bifurcations of synchronous periodic orbits. As will be seen below, in the case of global coupling, the stability region of a synchronous periodic orbit in the parameter plane is the same, independently of N, while for the other nonglobal-coupling cases it depends on the coupling range K.

The surface of section for the system of the coupled MO's (4b) is the time-1 map. Hence the maps of an initial orbit point $\mathbf{z}(0)$ $[= (z_1(0), \ldots, z_N(0))]$ can be computed by sampling the orbits points $\mathbf{z}(m)$ at the discrete time $t = m$ $(m = 1, 2, 3, \ldots)$. We will call the transformation $\mathbf{z}(m) \to \mathbf{z}(m+1)$ the Poincaré map and write $\mathbf{z}(m+1) = P(\mathbf{z}(m))$. Linear stability and bifurcations of a synchronous orbit with period q in the Poincaré map P such that $P^q(\mathbf{z}(0)) = \mathbf{z}(0)$ will be discussed below. (Here P^k means the k-times iterated map.)

The stability analysis of an orbit in coupled MO's can be conveniently carried out by Fourier-transforming with respect to the discrete space $\{m\}$.[13] Consider an orbit $\{x_m(t); m = 1, \ldots, N\}$ in the system of N coupled MO's (2). The discrete spatial Fourier transform of the orbit is

$$\mathcal{F}[x_m(t)] \equiv \frac{1}{N}\sum_{m=1}^{N} e^{-2\pi i m j/N} x_m(t) = \xi_j(t)\,, \qquad j = 0, 1, \ldots, N-1\,. \tag{12}$$

The Fourier transform $\xi_j(t)$ satisfies $\xi_j^*(t) = \xi_{N-j}(t)$ ($*$ denotes complex conjugate) and the wavelength of a mode with index j is N/j for $j \le N/2$ and $N/(N-j)$ for $j > N/2$.

To determine the stability of a synchronous q-periodic orbit $[x_1(t) = \cdots = x_N(t) \equiv x^*(t)$ for all t and $x^*(t) = x^*(t+q)]$, we consider an infinitesimal perturbation $\{\delta x_m(t)\}$ to the synchronous orbit, i.e., $x_m(t) = x^*(t) + \delta x_m(t)$ for $m = 1, \ldots, N$. Linearizing the governing equation (2) for the system of N coupled MO's at the synchronous orbit, we have

$$\delta\ddot{x}_m = \frac{\partial f(x^*, \dot{x}^*, t)}{\partial x^*}\delta x_m + \frac{\partial f(x^*, \dot{x}^*, t)}{\partial \dot{x}^*}\delta\dot{x}_m + \sum_{l=1}^{N} G_l(x^*)\delta x_{l+m-1}\,, \tag{13}$$

where

$$G_l(x) \equiv \left.\frac{\partial g(x_1, \ldots, x_N)}{\partial x_l}\right|_{x_1=\cdots=x_N=x}\,. \tag{14}$$

Hereafter the functions G_l's will be called "reduced" coupling functions of $g(x_1, \ldots, x_N)$.

Let $\delta\xi_j(t)$ be the Fourier transform of $\delta x_m(t)$, i.e.,

$$\delta\xi_j = \mathcal{F}[\delta x_m(t)] = \frac{1}{N}\sum_{m=1}^{N} e^{-2\pi i m j/N}\delta x_m\,, \quad j = 0, 1, \ldots, N-1\,. \tag{15}$$

Here $\delta\xi_0$ is the synchronous-mode perturbation and all the other $\delta\xi_j$'s with nonzero indices j are the asynchronous-mode perturbations. Then the Fourier transform of Eq. (13) becomes

$$\delta\ddot{\xi}_j = \frac{\partial f(x^*,\dot{x}^*,t)}{\partial \dot{x}^*}\delta\dot{\xi}_j + \left[\frac{\partial f(x^*,\dot{x}^*,t)}{\partial x^*} + \sum_{l=1}^{N} G_l(x^*)e^{2\pi i(l-1)j/N}\right]\delta\xi_j\,, \qquad j = 0,1,\ldots,N-1\,. \tag{16}$$

Note that all the modes $\delta\xi_j$'s become decoupled for the synchronous orbit.

Equation (16) can also be put into the following form

$$\begin{pmatrix} \delta\dot{\xi}_j \\ \delta\dot{\eta}_j \end{pmatrix} = L_j(t)\begin{pmatrix} \delta\xi_j \\ \delta\eta_j \end{pmatrix}, \qquad j = 0,1,\ldots,N-1\,, \tag{17}$$

where

$$L_j(t) = \begin{pmatrix} 0 & 1 \\ \dfrac{\partial f(x^*,\dot{x}^*,t)}{\partial x^*} + \displaystyle\sum_{l=1}^{N} G_l(x^*)e^{2\pi i(l-1)j/N} & \dfrac{\partial f(x^*,\dot{x}^*,t)}{\partial \dot{x}^*} \end{pmatrix}. \tag{18}$$

Note that each L_j is a q-periodic matrix, i.e., $L_j(t) = L_j(t+q)$. Let $\Phi_j(t) = (\phi_j^{(1)}(t), \phi_j^{(2)}(t))$ be a fundamental solution matrix with $\Phi_j(0) = I$. Here $\phi_j^{(1)}(t)$ and $\phi_j^{(2)}(t)$ are two independent solutions expressed in column vector forms and I is the 2×2 unit matrix. Then a general solution of the q-periodic system has the following form

$$\begin{pmatrix} \delta\xi_j(t) \\ \delta\eta_j(t) \end{pmatrix} = \Phi_j(t)\begin{pmatrix} \delta\xi_j(0) \\ \delta\eta_j(0) \end{pmatrix}, \qquad j = 0,1,\ldots,N-1\,. \tag{19}$$

Substitution of Eq. (19) into Eq. (17) leads to an initial-value problem to determine $\Phi_j(t)$,

$$\dot{\Phi}_j(t) = L_j(t)\Phi_j(t)\,, \qquad \Phi_j(0) = I\,. \tag{20}$$

Each 2×2 matrix M_j $[\equiv \Phi_j(q)]$, which is obtained through integration of Eq. (20) over the period q, determines the stability of the q-periodic synchronous orbit against the jth-mode perturbation.

The characteristic equation of each matrix M_j $(j = 0,1,\ldots,N-1)$ is

$$\lambda_j^2 - \mathrm{tr}\, M_j\, \lambda_j + \det M_j = 0\,, \tag{21}$$

where $\mathrm{tr}\, M_j$ and $\det M_j$ denote the trace and determinant of M_j, respectively. The eigenvalues, $\lambda_{j,1}$ and $\lambda_{j,2}$, of M_j are called the Floquet stability multipliers, which characterize the stability of the synchronous q-periodic orbit against the jth-mode perturbation. Since the $j = 0$ case corresponds to the synchronous mode, the first pair of stability multipliers $(\lambda_{0,1}, \lambda_{0,2})$ is called the pair of synchronous stability multipliers. On the other hand, all the other pairs of stability multipliers are called

the pairs of asynchronous stability multipliers, because all the other cases of $j \neq 0$ correspond to asynchronous modes.

By using the Liouville's formula,[14] we obtain the determinant of M_j,

$$\mathrm{Det}\, M_j = e^{-\Gamma q}\,. \tag{22}$$

Hence each pair of stability multipliers $(\lambda_{j,1}, \lambda_{j,2})$ $(j = 0, 1, \ldots, N-1)$ lies either on the circle of radius $e^{-\Gamma q/2}$, or on the real axis in the complex plane. The synchronous orbit is stable against the jth-mode perturbation when the pair of stability multipliers $(\lambda_{j,1}, \lambda_{j,2})$ lies inside the unit circle in the complex plane. We first note that the stability multipliers never cross the unit circle in the complex plane, except at the real axis and hence Hopf bifurcations do not occur. Consequently, it can lose its stability against the jth mode perturbation only when a stability multiplier λ_j decreases (increases) through $-1(1)$ on the real axis.

A more convenient real quantity R_j, called the residue and defined by

$$R_j \equiv \frac{1 + \det M_j - \mathrm{tr}\, M_j}{2(1 + \det M_j)}\,, \qquad j = 0, 1, \ldots, N-1\,, \tag{23}$$

was introduced in Ref. 15 to characterize stability of periodic orbits in two-dimensional dissipative maps with constant Jacobian determinants. Here the first one R_0 is associated with the stability against the synchronous-mode perturbation and hence it may be called the synchronous residue. On the other hand, all the other ones R_j $(j \neq 0)$ are called the asynchronous residues, because they are associated with the stability against the asynchronous-mode perturbations.

A synchronous periodic orbit is stable against the jth-mode perturbation when $0 < R_j < 1$ (i.e., the pair of stability multipliers $(\lambda_{j,1}, \lambda_{j,2})$ lies inside the unit circle in the complex plane). When R_j decreases through 0 (i.e., a stability multiplier λ_j increases through 1), the periodic orbit loses its stability via saddle-node or pitchfork bifurcation (PFB). On the other hand, when R_j increases through 1 (i.e., a stability multiplier λ_j decreases through -1), it becomes unstable via period-doubling bifurcation (PDB). We also note that $a(n)$ synchronous (asynchronous) bifurcation takes place for $j = 0$ $(j \neq 0)$. For each case of the synchronous (asynchronous) PFB and PDB, two type of supercritical and subcritical bifurcations occur. For the supercritical case of the synchronous (asynchronous) PFB and PDB, the synchronous periodic orbit loses its stability and gives rise to the birth of a pair of new stable synchronous (asynchronous) orbits with the same period and a new stable synchronous (asynchronous) period-doubled orbit, respectively. However, for the subcritical case of the synchronous (asynchronous) PFB and PDB, the synchronous periodic orbit becomes unstable by absorbing a pair of unstable synchronous (asynchronous) orbits with the same period and an unstable synchronous (asynchronous) period-doubled orbit, respectively. (For more details on bifurcatios, refer to Ref. 16.)

It follows from the condition (3) that the reduced coupling functions of Eq. (14) satisfy

$$\sum_{l=1}^{N} G_l(x) = 0\,. \tag{24}$$

Hence the matrix (18) for $j = 0$ becomes

$$L_0(t) = \begin{pmatrix} 0 & 1 \\ \dfrac{\partial f(x^*, \dot{x}^*, t)}{\partial x^*} & \dfrac{\partial f(x^*, \dot{x}^*, t)}{\partial \dot{x}^*} \end{pmatrix}. \tag{25}$$

This is just the linearized Poincaré map of the uncoupled MO.[9] Hence the synchronous residue R_0 becomes the same as the residue of the uncoupled MO, i.e., it depends only on the amplitude A. While there is no coupling effect on R_0, the coupling affects all the other asynchronous residues R_j $(j \neq 0)$.

In case of the global coupling of Eq. (11), the reduced coupling functions become:

$$G_l(x) = \begin{cases} (1-N)G(x) & \text{for } l = 1 \\ G(x) & \text{for } l \neq 1, \end{cases} \tag{26}$$

where $G(x) = (c/N)u'(x)$. Substituting G_l's into the second term of the $(2,1)$ entry of the matrix $L_j(t)$ of Eq. (18), we have:

$$\sum_{l=1}^{N} G_l(x) e^{2\pi i(l-1)j/N} = \begin{cases} 0 & \text{for } j = 0, \\ -cu'(x) & \text{for } j \neq 0. \end{cases} \tag{27}$$

Hence all the asynchronous residues R_j $(j \neq 0)$ become the same, i.e., $R_1 = \cdots = R_{N-1}$. Consequently there exist only two independent residues R_0 and R_1, independently of N.

We next consider the non-global coupling of the form (10) and define

$$G(x) \equiv \frac{c}{2K+1} u'(x)\,, \tag{28}$$

where $1 \leq K \leq \frac{N-2}{2}$ $(\frac{N-3}{2})$ for even (odd) N larger than 3. Then we have

$$G_l(x) = \begin{cases} -2KG(x) & \text{for } l = 1, \\ G(x) & \text{for } 2 \leq l \leq 1+K \text{ or} \\ & \text{for } N+1-K \leq l \leq N, \\ 0 & \text{otherwise.} \end{cases} \tag{29}$$

Substituting the reduced coupling functions into the matrix $L_j(t)$, the second term of the $(2,1)$ entry of $L_j(t)$ becomes:

$$\sum_{l=1}^{N} G_l(x) e^{2\pi i(l-1)j/N} = -S_N(K,j) c u'(x)\,, \tag{30}$$

where

$$S_N(K,j) \equiv \frac{4}{2K+1}\sum_{k=1}^{K}\sin^2\left(\frac{\pi jk}{N}\right) = 1 - \frac{\sin(2K+1)(\pi j/N)}{(2K+1)\sin(\pi j/N)}\,. \tag{31}$$

Hence, unlike the global-coupling case, all the asynchronous residues vary depending on the coupling range K as well as on the mode number j. Since $S_N(K,j) = S_N(K,N-j)$, the residues satisfy

$$R_j = R_{N-j}\,, \qquad j = 0,1,\ldots,N-1\,. \tag{32}$$

Thus it is sufficient to consider only the case of $0 \le j \le \frac{N}{2}$ ($\frac{N-1}{2}$) for even (odd) N. Comparing the expression in Eq. (30) with that in Eq. (27) for $j \neq 0$, one can easily see that they are the same except for the factor $S_N(K,j)$. Consequently, making a change of the coupling parameter $c \to \frac{c}{S_N(K,j)}$, the residue R_j for the non-global coupling case of range K becomes the same as that for the global-coupling case.

When the synchronous residue R_0 of a synchronous periodic orbit increases through 1, the synchronous orbit loses its stability via synchronous period-doubling bifurcation, giving rise to the birth of a new synchronous period-doubled orbit. Here we are interested in such synchronous period-doubling bifurcations. Thus, for each mode with nonzero index j we consider a region in the $A-c$ plane, in which the synchronous orbit is stable against the perturbations of both modes with indices 0 and j. This stable region is bounded by four bifurcation curves determined by the equations $R_0 = 0$, 1 and $R_j = 0$, 1 and it will be denoted by U_N.

For the case of global coupling, those stable regions coincide, irrespectively of N and j, because all the asynchronous residues R_j's ($j \neq 0$) are the same, independently of N. The stable region for this global-coupling case will be denoted by U_G. Note that U_G itself is just the stability region of the synchronous orbit, irrespectively of N, because the synchronous orbit is stable against the perturbations of all synchronous and asynchronous modes in the region U_G. Thus the stability diagram of synchronous orbits of period 2^n ($n = 0,1,2,\ldots$) in the $A-c$ plane becomes the same, independently of N.

However, the stable region U_N varies depending on the coupling range K and the mode number j for the nonglobal-coupling cases, i.e., $U_N = U_N(K,j)$. To find the stability region of a synchronous orbit in the N coupled MO's with a given K, one may start with the stability region U_G for the global-coupling case. Rescaling the coupling parameter c by a scaling factor $1/S_N(K,j)$ for each nonzero j, the stable region U_G is transformed into a stable region $U_N(K,j)$. Then the stability region of the synchronous orbit is given by the intersection of all such stable regions U_N's.

Finally, we briefly discuss Lyapunov exponents of a synchronous orbit in the Poincaré map P, characterizing the mean exponential rate of divergence of nearby orbits.[17] As shown in Eq. (16), all the synchronous and asychronous modes of a perturbation to a synchronous orbit becomes decoupled. Hence each matrix M_j [$\equiv \Phi_j(1)$] with $q = 1$ determines the pair of Lyapunov exponents $(\sigma_{j,1}, \sigma_{j,2})$

$(j = 0, 1, \ldots, N-1)$, characterizing the average exponential rates of divergence of the jth mode perturbation, where $\sigma_{j,1} \geq \sigma_{j,2}$. Since each M_j has the same constant Jacobian determinant (i.e., $\det M_j = e^{-\Gamma}$), each pair of Lyapunov exponents satisfies $\sigma_{j,1} + \sigma_{j,2} = -\Gamma$. Note also that the first pair of synchronous Lyapunov exponents is just the pair of the Lyapunov exponents of the uncoupled MO,[9] and the coupling affects only all the other pairs of asynchronous Lyapunov exponents.

3. Critical Scaling Behaviors for the Case of Global Coupling

In this section, by varying the two parameters A and c, we study the critical scaling behaviors of synchronous PDB's in the N globally-coupled MO's for a moderately damped case of $\Gamma = 1.38$. It is found that the zero-coupling critical point and an infinity of critical line segments constitute the same critical set, independently of N. Three kinds of critical behaviors associated with the scaling of the coupling parameter c are found on the critical set, while the critical scaling behavior of the driving amplitude A is always the same as those in the uncoupled MO.[9] Note also that the structure of the critical set and the critical scaling behaviors are the same as those for the abstract system of the coupled 1D maps.[12]

As shown in Sec. 2, a synchronous periodic orbit is stable when all its residues R_j $(j = 0, 1, \ldots, N-1)$ defined in Eq. (23) lie between 0 and 1 (i.e., $0 < R_j < 1$). Here R_0 is the synchronous residue determining the stability against the synchronous-mode perturbation, while all the other ones R_j $(j \neq 0)$ are the asynchronous residues determining the stability against the asynchronous-mode perturbations. For the globally-coupled case, all the asynchronous residues become the same, independently of j, and hence only one independent asynchronous residue (e.g., R_1) exists. Accordingly, the stability region of a synchronous periodic orbit becomes bounded by four bifurcation lines determined by the equations $R_0 = 0, 1$ and $R_1 = 0, 1$. Here the $R_0 = 0$ and 1 ($R_1 = 0$ and 1) lines correspond to the synchronous (asynchronous) PFB and PDB lines, respectively. In such a way, we obtain the stability diagram of the synchronous 2^n-periodic orbits $(n = 0, 1, 2, \ldots)$ in the $A - c$ plane. Note also that the stability diagram becomes the same, independently of N, because all the asynchronous residues R_j $(j \neq 0)$ for each synchronous orbit are also the same, irrespectively of N. Consequently, the structure of the critical set and the critical behaviors for the global-coupling case become the same, independently of N.

As an example, we consider a linearly coupled case in which the coupling function (11) is

$$g(x_1, \ldots, x_N) = c \left[\frac{1}{N} \sum_{m=1}^{N} x_m - x_1 \right] . \tag{33}$$

Figure 1(a) shows the stability diagram of the synchronous orbits with low period $q = 1, 2$ for this linearly-coupled case. The stable region of a synchronous orbit is bounded by its PDB and PFB lines. The horizontal (non-horizontal) solid and

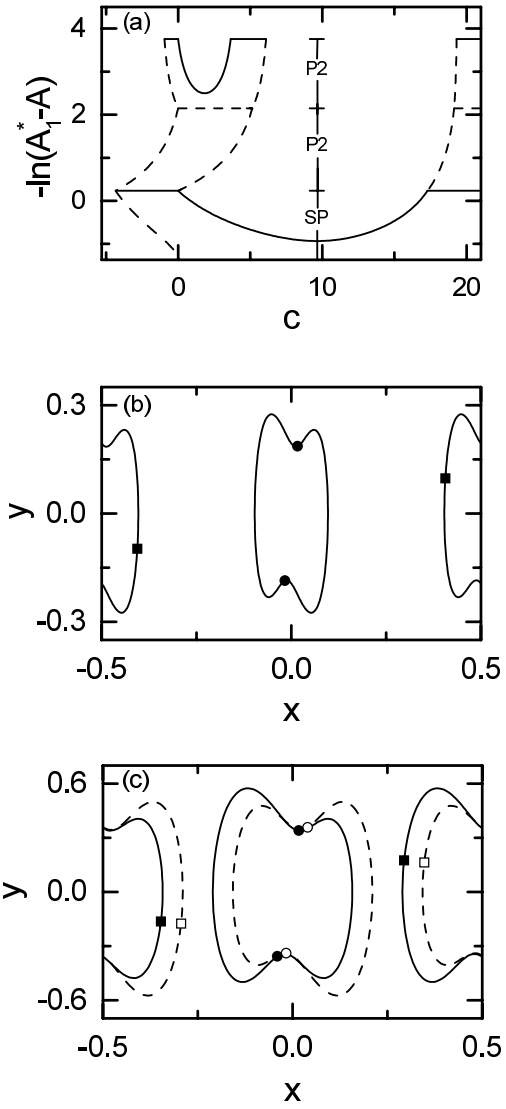

Fig. 1. (a) Stability diagram of the synchronous orbits of low period $q = 1, 2$ in N linearly coupled MO's with the global coupling. Here $A_1^*(= 3.934\,787\ldots)$ is the first period-doubling transition point of the uncoupled MO. The stable regions of the two stationary points, S_1-symmetric orbits with period 2 and S_1-asymmetric orbits with period 2 are denoted by the SP, the lower P2 and the upper P2, respectively. The horizontal (non-horizontal) solid and dashed boundary lines correspond to synchronous (asynchronous) PDB and PFB lines, respectively. (b) Phase portraits for $A = 3.31$. The phase flows of two S_1-symmetric orbits with period 2 born via synchronous supercritical PDB's are denoted by solid curves and its Poincaré maps are represented by solid symbols (circle and square). (c) Phase portraits for $A = 3.87$. Two conjugate pairs of S_1-asymmetric orbits with period 2 born via synchronous supercritical PFB's are shown. For each S_1-conjugate pair, the phase flow (Poincaré map) of one orbit is denoted by a solid curve [solid symbol (circle or square)], while the that of the other one is represented by a dashed curve [open symbol (circle or square)]. See the text for other details.

dashed boundary lines correspond to synchronous (asynchronous) PDB and PFB lines, respectively. (Each bifurcation may be supercritical or subcritical.) Note also that the horizontal synchronous PDB or PFB lines extend to the (plus) infinity ($c = \infty$). For the sake of convenience, only some parts (up to $c = 21$) of the infinitely long lines are drawn in the figure.

We first consider the bifurcations associated with stability of the synchronous stationary points. [A synchronous orbit $(z_1, \ldots, z_N)$ satisfies $z_1(t) = \cdots = z_N(t) \equiv z^*(t) = (x^*(t), y^*(t))$.] As shown in the uncoupled MO,[9] there are two stationary points. For the first stationary point $z_{\rm I}^* = (0, 0)$ and for the second one $z_{\rm II}^* = (\frac{1}{2}, 0)$. These two stationary points are symmetric ones with respect to the inversion symmetry S_1, while they are asymmetric and conjugate ones with respect to the shift symmetry S_2. Hence they are partially symmetric orbits with only the inversion symmetry S_1. Since the conjugate orbits have the same stability multipliers, the stability regions of the two stationary points become the same. Their stability region is denoted by the SP in Fig. 1(a). Note that the SP is U-shaped, because a parabolalike asynchronous PDB line also is a boundary line of the SP. An asynchronous supercritical PDB occurs at the parabolalike solid line, whereas an asynchronous subcritical PFB takes place at the non-horizontal dashed line. However, each synchronous stationary point becomes unstable via synchronous supercritical PDB when the horizontal solid line is crossed. Consequently, two new stable synchronous S_1-symmetric orbits with period 2 appear and their stable region is denoted by the lower P2 in Fig. 1(a). An example for $A = 3.31$ is shown in Fig. 1(b). Like the stationary points, these two stable period-doubled orbits with the inversion symmetry S_1, whose phase flows are denoted by solid curves, are asymmetric and conjugate ones with respect to the shift symmetry S_2. The Poincaré map of the stable 2-periodic orbit encircling the unstable stationary point $z_{\rm I}^*$ ($z_{\rm II}^*$) is also represented by a solid circle (square). Each S_1-symmetric 2-periodic orbit loses its stability through asynchronous PFB's when crossing the nonhorizontal dashed boundary curves. However, it becomes unstable via synchronous supercritical (symmetry-breaking) PFB when the horizonatl dashed line is crossed. Consequently, two pairs of new stable synchronous S_1-asymmetric orbits with the same period 2 appear and their stable region is denoted by the upper P2 in Fig. 1(a). An example for $A = 3.87$ is given in Fig. 1(c). One S_1-conjugate pair encircles the unstable stationary point $z_{\rm I}^*$, while the other pair encircles the unstable stationary point $z_{\rm II}^*$. For each S_1-conjugate pair, the phase flow [Poincaré map] of one orbit is denoted by a solid line [solid symbol (circle or square)], whereas that of the other one is represented by a dashed line [open symbol (circle or square)]. We also note that each synchronous S_1-asymmetric 2-periodic orbit becomes unstable via synchronous supercritical PDB when the horizontal solid line of its stable region is crossed and gives rise to the birth of a new synchronous S_1-asymmetric 4-periodic orbit. Here we are interested in such synchronous supercritical PDB's.

Figure 2 shows the stability diagram of synchronous S_1-asymmetric orbits born by synchronous supercritical PDB's. Each synchronous S_1-asymmetric orbit of level

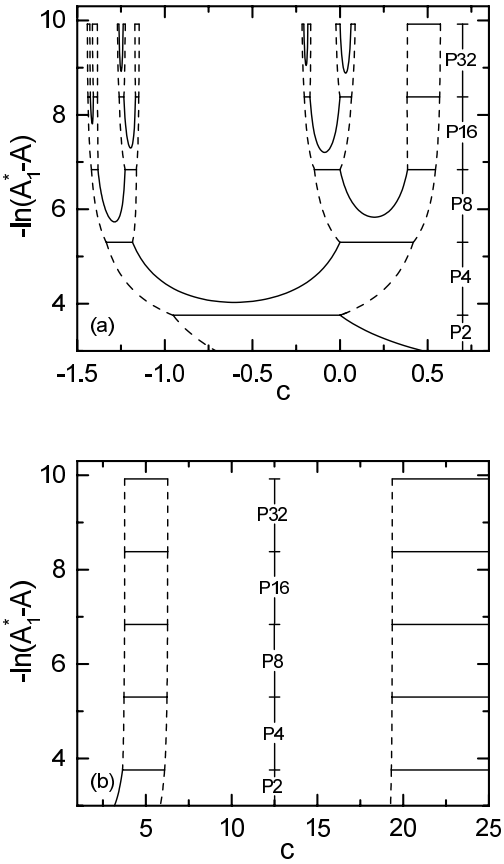

Fig. 2. Stability diagram of synchronous S_1-asymmetric 2^n-periodic ($n = 1, 2, 3, 4, 5$) orbits of level n born via synchronous supercritical PDB's. PN denotes the stable region of an S_1-asymmetric orbit of period N ($N = 2, 4, 8, 16, 32$). The solid and dashed boundary lines represent the same as those in Fig. 1(a). The stability diagram starting from the leftmost (right two) side(s) of the P2 is shown in (a) [(b)]. Note its treelike structure. See the text for other details.

n (period 2^n, $n = 1, 2, 3, \ldots$) loses its stability at the horizontal solid line of its stable region via synchronous supercritical PDB and gives rise to the birth of a synchronous S_1-asymmetric period-doubled orbit of level $n+1$. Such an infinite sequence ends at a finite value of $A_1^* = 3.934\,787\ldots$, which is the first period-doubling transition point of the uncoupled MO.[9] Consequently, a synchronous quasiperiodic orbit, whose maximum synchronous Lyapunov exponent is zero (i.e., $\sigma_{0,1} = 0$), exists on the $A = A_1^*$ line.

We examine the treelike structure of the stability diagram in Fig. 2(a), which consists of an infinite pile of U-shape regions and rectangular-shape regions. Note that the treelike structure is asymptotically the same as that in the coupled 1D maps.[12] The U-shape branching is repeated at one side of each U-shape region, including the $c = 0$ line segment. The branching side will be referred to as the zero

c side. However, the other side of each U-shape region grows like a chimney without any further branchings (as an example, see the left branch in Fig. 2(b) starting from the right side of the U-shape region in the upper P2). As in the coupled 1D maps,[12] this rule governs the asymptotic behavior of the treelike structure, even though there are a few exceptions for lower-level orbits. Other type of U-shape regions without the zero c sides [e.g., the leftmost U-shape region in the third-level stability region in Fig. 2(a)] may appear in the lower-level stability regions. However, the U-shape branching for this kind of U-shape region ends at some finite level and then each side of the U-shape region grows like a chimney without any further branchings. Consequently, an infinite number of successive branchings occur only for the case of the U-shape region with the zero c side.

A sequence of connected stability regions with increasing period is called a "period-doubling route".[12] There are two kinds of period-doubling routes. The sequence of the U-shape regions with the zero c sides converges to the zero-coupling point $c = 0$ on the $A = A_1^*$ line. It will be referred to as the U route. On the other hand, a sequence of rectangular regions in each chimney converges to a critical line segment on the $A = A_1^*$ line. For an example, the rightmost one in Fig. 2(a) is the line segment joining the left end point c_l $(= 0.385\,245\ldots)$ and the right end point c_r $(= 0.574\,345\ldots)$ on the $A = A_1^*$ line. This kind of route will be called a C route. Note that there are infinitely many C routes, while the U route converging to the zero-coupling critical point $(A_1^*, 0)$ is unique. Hence an infinite number of critical line segments, together with the zero-coupling critical point, constitute the critical set.

We now study the critical scaling behaviors on the critical set. First, consider the case of the U route ending at the zero-coupling critical point. We follow the synchronous orbits of period $q = 2^n$ up to level $n = 9$ in the U route and obtain a self-similar sequence of parameters (A_n, c_n), at which each synchronous orbit of level n has some given synchronous and asynchronous residues $R_0 = 1$ and $R_1 = 0$. Then the sequence $\{(A_n, c_n)\}$ converges geometrically to the zero-coupling critical point $(A_1^*, 0)$. As in the uncoupled MO,[9] the sequence $\{A_n\}$ obeys the one-term scaling law,

$$\Delta A_n \sim \delta^{-n} \qquad \text{for large } n\,, \tag{34}$$

where $\Delta A_n = A_n - A_{n-1}$ and $\delta \simeq 4.67$. The value of the scaling factor δ of the amplitude A agrees well with the Feigenbaum constant $(= 4.669\ldots)$ of the 1D map.[11] On the other hand, the sequence $\{c_n\}$ obeys a two-term scaling law,

$$\Delta c_n \sim C_1 \mu_1^{-n} + C_2 \mu_2^{-n} \qquad \text{for large } n\,, \tag{35}$$

where $\Delta c_n = c_n - c_{n-1}$, $|\mu_2| > |\mu_1|$ and C_1 and C_2 are some constants. Equation (35) gives

$$\Delta c_n = s_1 \Delta c_{n+1} - s_2 \Delta c_{n+2}\,, \tag{36}$$

Table 1. For the case of the U route, the scaling factors $\mu_{1,n}$ and $\mu_{2,n}$ in the two-term scaling for the coupling parameter are shown in the second and third columns, respectively. A product of them, $\mu_{1,n}^2/\mu_{2,n}$, is shown in the fourth column.

n	$\mu_{1,n}$	$\mu_{2,n}$	$\mu_{1,n}^2/\mu_{2,n}$
4	−2.501	3.00	2.08
5	−2.504	3.16	1.99
6	−2.505	3.13	2.01
7	−2.504	3.11	2.02

where $s_1 = \mu_1 + \mu_2$ and $s_2 = \mu_1\mu_2$. We first obtain s_1 and s_2 of level n from Δc_n's:

$$s_{1,n} = \frac{\Delta c_n \Delta c_{n+1} - \Delta c_{n-1}\Delta c_{n+2}}{\Delta c_{n+1}^2 - \Delta c_n \Delta c_{n+2}}\,, \qquad s_{2,n} = \frac{\Delta c_n^2 - \Delta c_{n+1}\Delta c_{n-1}}{\Delta c_{n+1}^2 - \Delta c_n \Delta c_{n+2}}\,. \tag{37}$$

Then the scaling factors $\mu_{1,n}$ and $\mu_{2,n}$ of level n are given by the solutions of the following quadratic equation,

$$\mu_n^2 - s_{1,n}\mu_n + s_{2,n} = 0\,. \tag{38}$$

Three sequences $\{\mu_{1,n}\}$, $\{\mu_{2,n}\}$ and $\{\mu_{1,n}^2/\mu_{2,n}\}$ are shown in Table 1. The second column shows rapid convergence of the first scaling factor $\mu_{1,n}$ to its limit value μ_1 ($\simeq -2.50$), which agrees well with the coupling-parameter scaling factor α ($= -2.502\ldots$) for the coupled 1D maps near the zero-coupling critical point.[12] It has been also shown in Ref. 12 that the scaling factor α is just the first relevant "coupling eigenvalue" (CE) ν_1 of the zero-coupling fixed map of the renormalization transformation for the case of the coupled 1D maps. In addition to $\nu_1 = \alpha$, the zero-coupling fixed map has another second relevant CE ν_2 ($= 2$), which also affects the scaling associated with coupling in the coupled 1D maps.[18] We thus consider the effect of the 2nd relevant CE on the scaling of the coupling parameter c. The second scaling factor $\mu_{2,n}$ seems to converge slowly to its limit value μ_2 ($\simeq 3.1$), whose accuracy is lower than that of μ_1. It seems from the third and fourth columns that the second scaling factor μ_2 may be expressed by a product of two relevant CE's ν_1 ($= \alpha$) and ν_2 ($= 2$),

$$\mu_2 = \frac{\nu_1^2}{\nu_2}\,. \tag{39}$$

It has been known that every scaling factor in the multiple-scaling expansion of a parameter is expressed by a product of the eigenvalues of a linearized renormalization operator.[19]

We also study the coupling effect on the asynchronous residue $R_{1,n}$ of the synchronous orbit of period 2^n near the zero-coupling critical point $(A_1^*, 0)$. Figure 3 shows three plots of $R_{1,n}(A_1^*, c)$ versus c for $n = 4, 5$ and 6. For $c = 0$, $R_{1,n}$ converges to a constant R_1^* ($= 1.300\,59\ldots$), called the critical asynchronous residue,

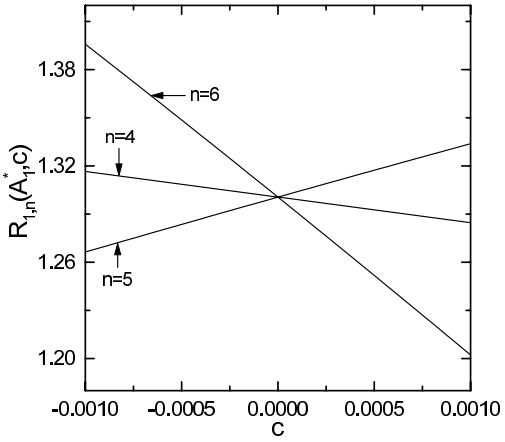

Fig. 3. Plots of the asynchronous residue $R_{1,n}(A_1^*, c)$ versus c near the zero-coupling critical point for $n = 4, 5, 6$.

as $n \to \infty$. However, when c is nonzero $R_{1,n}$ diverges as $n \to \infty$, i.e., its slope S_n $(\equiv (\partial R_{1,n}/\partial c)|_{(A_1^*,0)})$ at the zero-coupling critical point diverges as $n \to \infty$.

As in the scaling for the coupling parameter, the sequence $\{S_n\}$ also obeys a two-term scaling law,

$$S_n \sim D_1\nu_1^n + D_2\nu_2^n \qquad \text{for large } n\,, \tag{40}$$

where $|\nu_1| > |\nu_2|$. This equation gives

$$S_{n+2} = r_1 S_{n+1} - r_2 S_n\,, \tag{41}$$

where $r_1 = \nu_1 + \nu_2$ and $r_2 = \nu_1\nu_2$. We first obtain r_1 and r_2 of level n from S_n's:

$$r_{1,n} = \frac{S_{n+1}S_n - S_{n+2}S_{n-1}}{S_n^2 - S_{n+1}S_{n-1}}\,, \qquad r_{2,n} = \frac{S_{n+1}^2 - S_nS_{n+2}}{S_n^2 - S_{n+1}S_{n-1}}\,. \tag{42}$$

Then the scaling factors $\nu_{1,n}$ and $\nu_{2,n}$ of level n are given by the roots of the quadratic equation,

$$\nu_n^2 - r_{1,n}\nu_n + r_{2,n} = 0\,. \tag{43}$$

They are listed in Table 2 and converge to constants ν_1 $(\simeq -2.503)$ and ν_2 $(\simeq 2)$ as $n \to \infty$, whose accuracies are higher than those of the coupling-parameter scaling factors. Note that the values of ν_1 and ν_2 agree well with those of the two relevant CE's ν_1 and ν_2 of the zero-coupling fixed map.

We next consider the cases of C routes, each of which converges to a critical line segment. Two kinds of additional critical behaviors are found at each critical line segment; the one critical behavior exists at both ends and the other critical behavior exists at interior points. In each C route, there are two kinds of self-similar sequences of parameters (A_n, c_n), at which each synchronous orbit of level n has some given residues R_0 and R_1; the one converges to the left end point

Table 2. The scaling factors $\nu_{1,n}$ and $\nu_{2,n}$ in the two-term scaling for the slope S_n of the asynchronous residue $R_{1,n}$ at the zero-coupling critical point are shown in the second and third columns, respectively.

n	$\nu_{1,n}$	$\nu_{2,n}$
4	−2.503	1.998
5	−2.503	2.000
6	−2.503	1.996
7	−2.502	2.001

of the critical line segment and the other converges to the right end point. As an example, consider the rightmost C route in Fig. 2(a), which converges to the critical line segment with two ends (A_1^*, c_l) and (A_1^*, c_r), where $c_l = 0.385\,245\ldots$ and $c_r = 0.574\,345\ldots$ We follow, in the rightmost C route, two self-similar sequences of parameters, one converging to the left end and the other converging to the right end. In both cases, the sequence $\{A_n\}$ converges geometrically to its accumulation value A_1^* with the 1D scaling factor δ ($\simeq 4.67$) like the case of the U route,

$$\Delta A_n \sim \delta^{-n} \qquad \text{for large } n\,, \tag{44}$$

where $\Delta A_n = A_n - A_{n-1}$. The sequences $\{c_n\}$ for both cases also obey the one-term scaling law,

$$\Delta c_n \sim \mu^{-n} \qquad \text{for large } n\,, \tag{45}$$

where $\Delta c_n = c_n - c_{n-1}$. The sequence of the scaling factor μ_n of level n is listed in Table 3 and converges to its limit value μ ($\simeq 2$). We also note that the value of μ agrees well with that of the coupling-parameter scaling factor ($\nu = 2$) of the coupled 1D maps near both ends of each critical line segment.[12] It has been also shown in Ref. 12 that the scaling factor ν ($= 2$) is just the only relevant CE of a

Table 3. We followed, in the rightmost C route in Fig. 2(a), two self-similar sequences of parameters (A_n, c_n), at which the pair of synchronous and asynchronous residues $(R_{0,n}, R_{1,n})$ of the synchronous orbit with period 2^n is (1, 0.1). They converge to both ends (A_1^*, c_l) and (A_1^*, c_r) of the critical line segment, where $A_1^* = 3.934\,787\ldots$, $c_l = 0.385\,245\ldots$ and $c_r = 0.574\,345\ldots$ The scaling factors of the coupling parameter at the left and right ends are shown in the second and third columns, respectively. In both cases the scaling factors seem to converge to the same limit value $\mu \simeq 2$.

n	μ_n	μ_n
5	1.53	3.09
6	1.87	2.59
7	1.90	2.27
8	1.96	2.12

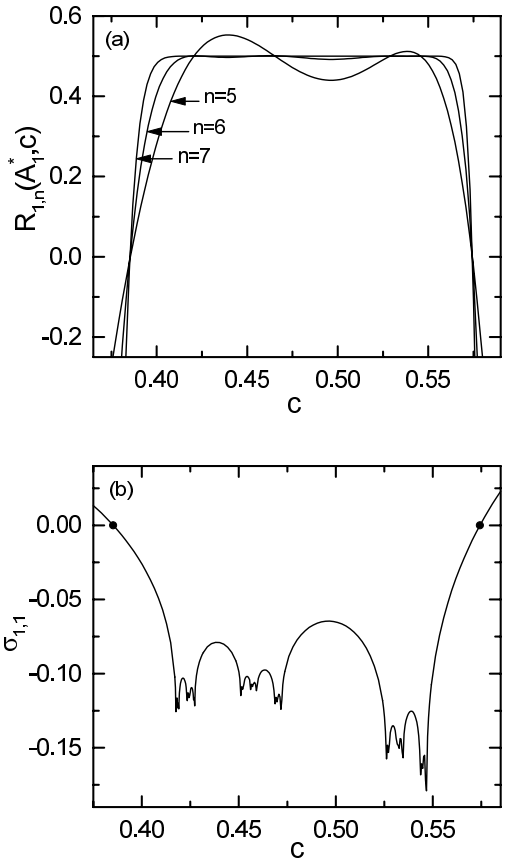

Fig. 4. (a) Plots of the asynchronous residue $R_{1,n}(A_1^*, c)$ versus c near the rightmost critical line in Fig. 2(a) for $n = 5, 6, 7$. (b) Plot of the maximum asynchronous Lyapunov exponent $\sigma_{1,1}$ of the synchronous quasiperiodic orbit near the rightmost critical line in Fig. 2(a). This plot consists of 200 c values, each of which is obtained by iterating the Poincaré map P 20 000 times to eliminate transients and then averaging over another 20 000 iterations. The values of $\sigma_{1,1}$ at both ends of the rightmost critical line are zero, which are denoted by solid circles.

nonzero-coupling fixed map of the renormalization transformation, governing the critical scaling behaviors at both ends for the case of the coupled 1D maps.

Figure 4(a) shows the behavior of the asynchronous residue $R_{1,n}(A_1^*, c)$ of the synchronous orbit of period 2^n near the rightmost critical line segment in Fig. 2(a). For $c = c_l$ and c_r, $R_{1,n}$ converges to a critical residue R_1^* $(= 0)$ as $n \to \infty$, which is different from that for the zero-coupling case. The slopes S_n's of $R_{1,n}$ at both ends obey well the one-term scaling law,

$$S_n \sim \nu^n \qquad \text{for large } n\,. \tag{46}$$

The two sequences of the scaling factors ν_n of level n at both ends are listed in Table 4 and converge to their limit values $\nu \simeq 2$, which agrees well with that of the only relevant CE $(\nu = 2)$ of the nonzero-coupling fixed map, governing

Table 4. The scaling factors ν_n's in the one-term scaling for the slopes S_n's of the asynchronous residue $R_{1,n}$ at the left and right ends of the rightmost critical line segment in Fig. 2(a) are shown in the second and third columns, respectively.

n	ν_n	ν_n
4	2.199	1.999
5	1.969	1.998
6	2.006	2.001
7	1.999	2.000
8	2.000	2.000

the critical scaling behaviors at both ends for the case of the coupled 1D maps. However, for any fixed value of c inside the critical line segment, $R_{1,n}$ converges to a critical residue R_1^* $(= 0.5)$ as $n \to \infty$ [see Fig. 4(a)]. This superstable case of $R_1^* = 0.5$ corresponds to the supercritical case of $\lambda_1^* = 0$ (λ_1^*: the critical asynchronous stability multiplier) for the coupled 1D maps,[12] because Eq. (23) of R for the case of 2D maps reduces to the equation of $R = 0.5 \times (1 - \lambda)$ for the case of 1D maps. We also note that as in the case of the coupled 1D maps, there exists no scaling factor of the coupling parameter inside the critical line segment and hence the coupling parameter becomes an irrelevant one at interior critical points. Thus, the critical behavior inside the critical line segment becomes the same as that of the uncoupled MO (i.e., that of the 1D map), which will be discussed in more details below. This kind of 1D-like critical behavior was found to be governed by another nonzero-coupling fixed map with no relevant CE for the case of the coupled 1D maps.[12]

There exists a synchronous quasiperiodic orbit on the $A = A_1^*$ line. As mentioned in Sec. 2, its synchronous Lyapunov exponents are the same as the Lyapunov exponents of the uncoupled MO, i.e., $\sigma_{0,1} = 0$ and $\sigma_{0,2} = -\Gamma$ $(= -1.38)$. The coupling affects only the second pair of asynchronous Lyapunov exponents $(\sigma_{1,1}, \sigma_{1,2})$, characterizing the mean exponential rate of divergence of the asynchronous mode of a nearby orbit. The maximum asynchronous Lyapunov exponent $\sigma_{1,1}$ near the rightmost critical line segment in Fig. 2(a) is shown in Fig. 4(b). Inside the critical line segment $(c_l < c < c_r)$, the synchronous quasiperiodic orbit on the synchronous plane becomes a synchronous attractor with $\sigma_{1,1} < 0$. Since the dynamics on the synchronous attractor is the same as that of the uncoupled MO, the critical systems of the coupled MO's at interior points exhibit essentially 1D-like critical scaling behaviors, because the critical scaling behaviors of the uncoupled MO are the same as those of the 1D maps.[9] However, as the coupling parameter c passes through c_l and c_r, the maximum asynchronous Lyapunov exponent $\sigma_{1,1}$ of the synchronous quasiperiodic orbit increases from zero and hence the coupling leads to desynchronization of the interacting system. Thus the synchronous quasiperiodic orbit ceases

to be an attractor outside the critical line segment and the system of the coupled MO's is asymptotically attracted to another asynchronous attractor.

What happens beyond the first period-doubling transition point A_1^* is also interesting. As in the uncoupled MO,[9] with increasing the amplitute A further from $A = A_1^*$, the two stationary points with $z_{\rm I}^* = (0,0)$ and $z_{\rm II}^* = (\frac{1}{2},0)$, undergo a cascade of "resurrections", i.e., each stationary point will restabilize after it loses its stability, destabilize again and so forth *ad infinitum*. For each case of the resurrections, an infinite sequence of PDB's leading to chaos follows. Consequently, the coupled MO's exhibit multiple period-doubling transitions to chaos.

As an example of the multiple period-doubling transitions to chaos, we consider the first resurrection of the stationary points. Figure 5 shows the second stability diagram of the synchronous stationary points and S_1-asymmetric orbits of level n (period 2^n, $n = 0, 1, 2, 3, 4$) in the $A - c$ plane. When crossing the horizontal solid boundary line of its stability region, denoted by the SP, each unstable stationary point restabilizes with birth of a new unstable synchronous S_1-symmetric orbit with period 2 via synchronous subcritical PDB. This is the first resurrection of the stationary points. However, when the horizontal dashed boundary line of the SP is crossed, each stabilized stationary point becomes unstable via synchronous supercritical (symmetry-breaking) PFB, which results in the birth of a conjugate pair of S_1-asymmetric synchronous orbits with period 1. Then each synchronous S_1-asymmetric orbit of level n becomes unstable at the horizontal solid boundary line of its stability region via synchronous supercritical PDB and gives rise to the birth of a synchronous S_1-asymmetric period-doubled orbit of the next level $n+1$.

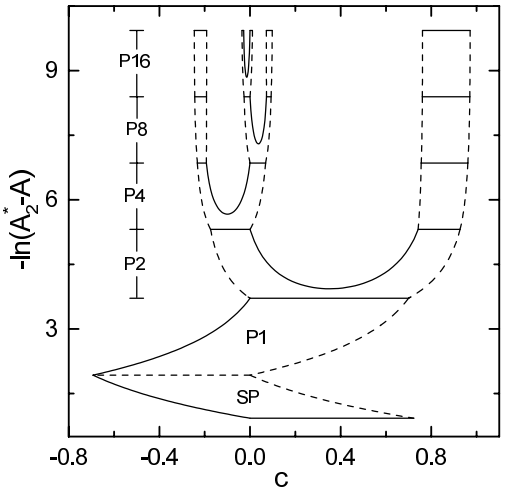

Fig. 5. Second stability diagram of the synchronous orbits near the $c = 0$ line. Here A_2^* ($= 24.148\,001\ldots$) is just the second period-doubling transition point of the uncoupled MO. The stable regions of the stationary points and the S_1-asymmetric N-periodic ($N = 1, 2, 4, 8, 16$) orbits are denoted by the SP and the PN, respectively. The solid and dashed boundary lines also represent the same as those in Fig. 1(a). For other details see the text.

Such an infinite sequence terminates at a finite value of $A_2^*(= 24.148\,001\ldots)$, which is the second period-doubling transition point of the uncoupled MO.[9] Note that the treelike structure of the stability diagram in Fig. 5 is essentially the same as that in Fig. 2(a). Hence the critical set also consists of an infinite number of critical line segments and the zero-coupling critical point, as in the first period-doubling transition case. In order to study the critical scaling behaviors on the critical set, we follow the synchronous S_1-asymmetric orbits up to level $n = 7$ in the U route and the rightmost C route. It is found that the critical scaling behaviors are the same as those for the first period-doubling transition case. That is, there exist three kinds of critical scaling behaviors at the zero-coupling critical point, both ends of each critical line segment and interior points.

In addition to the linear-coupling case (33), we have also studied two other nonlinear-coupling cases,

$$g(x_1,\ldots,x_N) = c\left[\frac{1}{N}\sum_{m=1}^{N} x_m^n - x_1^n\right], \quad n = 2,3\,. \tag{47}$$

As in the linear-coupling case, the zero-coupling critical point and an infinite number of critical line segments constitute the critical set for the quadratic and cubic coupling cases. Moreover, the critical scaling behaviors for these nonlinear-coupling cases are also found to be the same as those for the linear-coupling case.

4. Critical Scaling Behaviors for the Case of Nonglobal Coupling

In this section we study the nonglobal-coupling cases with the coupling range $K < N/2((N-1)/2)$ for even (odd) N. The structure of the critical set becomes different from that for the global-coupling case, because of a significant change in the stability diagram of the synchronous orbits with period 2^n $(n = 1, 2, 3, \ldots)$, as will be seen below.

As an example, we consider a linearly-coupled, nearest-neighbor coupling case with $K = 1$, in which the coupling function is

$$g(x_1,\ldots,x_N) = \frac{c}{3}(x_2 + x_N - 2x_1) \qquad \text{for } N > 3\,. \tag{48}$$

As shown in Sec. 2, the stable region U_N, in which a synchronous orbit is stable against the perturbations of both modes with indices 0 and j $(\neq 0)$, varies depending on the mode number j, because the asynchronous residue R_j $(j \neq 0)$ depends on j. To find the stability region of the synchronous orbit, one can start with the stability region U_G for the global-coupling case. Rescaling the coupling parameter c by a scaling factor $1/S_N(1,j)$ [$S_N(K,j)$ is given in Eq. (31)], the stable region U_G is transformed into a stable region $U_N(1,j)$. Then the stability region of the synchronous orbit is given by the intersection of all such stable regions U_N's.

As an example, we consider the case with $N = 4$. Figure 6 shows the stability regions of the synchronous S_1-asymmetric 2^n-periodic $(n = 1, 2, 3, 4)$ orbits. Note

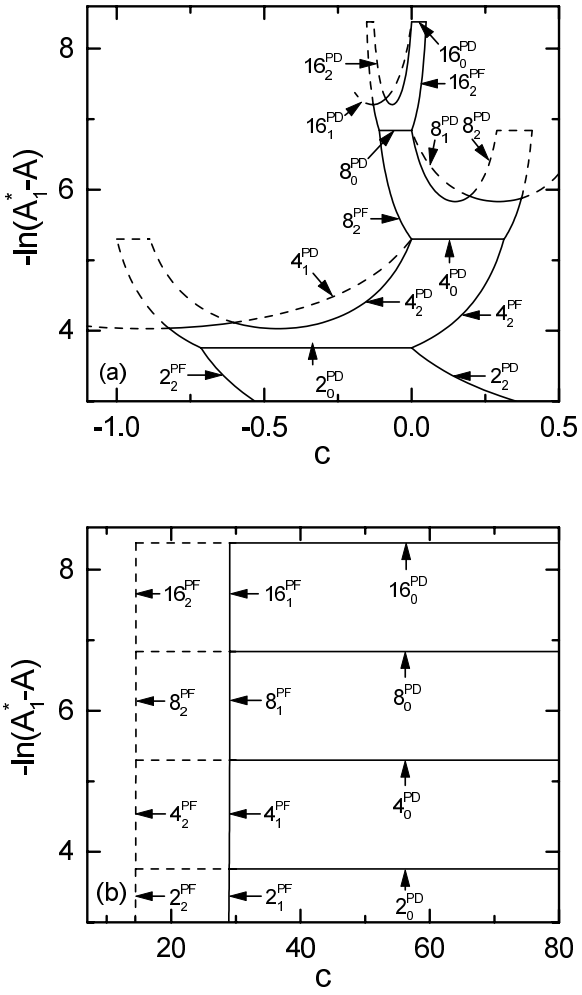

Fig. 6. Stability diagram of synchronous orbits in four linearly-coupled MO's with the nearest-neighbor coupling ($K = 1$). Each stable region is bounded by its solid boundary curves. For a synchronous orbit of period q, the PDB (PFB) curve of the mode with index j is denoted by a symbol $q_j^{PD(PF)}$. The stability diagrams starting from the left side of the U-shape region and from the rightmost rectangular region in the stability region of a synchronous S_1-asymmetric orbit with period 2 are shown in (a) and (b), respectively. For other details see the text.

that the scaling factor $1/S_4(1, j)$ has its minimum value $3/4$ at $j = 2$. However, for each synchronous orbit, $U_4(1, 2)$ itself cannot be the stability region, because bifurcation curves of different modes with nonzero indices intersect one another. We first examine the structure of the stability diagram in Fig. 6(a), starting from the left region in the stability region of the synchronous S_1-asymmetric orbit of level 1 ($n = 1$). For the case of level 2 ($n = 2$), the zero c side of $U_4(1, 2)$ including a $c = 0$ line segment remains unchanged, whereas the other side becomes flattened by

the bifurcation curve of the asynchronous mode with $j = 1$. Due to the successive flattening with increasing level n, a significant change in the stability diagram occurs. Of the infinite number of period-doubling routes for the global-coupling case, only the U route ending at the zero-coupling critical point remains. Thus only the zero-coupling point is left as a critical point in the parameter plane. However, as shown in Fig. 6(b), the rightmost branch of the stability diagram, starting from the rightmost rectangular region in the stability region of the synchronous S_1-asymmetric periodic orbit of level 1, is the same as that for the global-coupling case except that the coupling parameter c is rescaled with the maximum scaling factor $1/S_4(1,1)$ $(= 1.5)$ of the $j = 1$ mode. Hence the rightmost C route ending at a critical line segment is also left. Consequently, the critical set for this nearest-neighbor coupling case is composed of the zero-coupling critical point and one critical line segment.

Consider a self-similar sequence of parameters (A_n, c_n), at which the synchronous orbits of period 2^n has some given residues, in the U route for the global-coupling case. Rescaling the coupling parameter with the minimum scaling factor $1/S_4(1,2)$ $(= 0.75)$, the sequence is transformed into a self-similar one for the $N = 4$ case of nearest-neighbor coupling. Hence the critical scaling behavior near the zero-coupling critical point becomes the same as that for the global-coupling case. As mentioned above, the rightmost C route in Fig. 2(b) for the global-coupling case is also transformed into the C route in Fig. 6(b) for the nearest-neighbor coupling case by rescaling c with the maximum scaling factor $1/S_4(1,1)$ $(= 1.5)$. Hence the critical scaling behaviors at both ends and interior points of the critical line segment are also the same as those for the global-coupling case.

The results for the nearest-neighbor coupling case with $K = 1$ extends to all the other nonglobal-coupling cases with $1 < K < \frac{N}{2}(\frac{N-1}{2})$ for even (odd) N. For each nonglobal-coupling case with $K > 1$, we first consider a mode with index $j_{\min}$ for which the scaling factor $1/S_N(K, j)$ becomes the smallest one and the stability region $U_N(K, j_{\min})$ including a $c = 0$ line segment. Here the value of $j_{\min}$ varies depending on the range K. Like the $K = 1$ case, the zero c side of $U_N(K, j_{\min})$ including the $c = 0$ line segemnt remains unchanged, whereas the other side becomes flattened by the bifurcation curves of the other modes with nonzero indices. Thus the overall shape of the stability diagram, starting from the left zero c side of the stability region of the synchronous S_1-asymmetric 2-periodic orbit, becomes essentially the same as that for the nearest-neighbor coupling case. Consequently, only the U route ending at the zero-coupling critical point is left as a period-doubling route and the critical scaling behavior near the zero-coupling critical point is also the same as that for the global-coupling case. We next consider a mode with index $j_{\max}$ for which the scaling factor $1/S_N(K, j)$ becomes the largest one. Rescaling c with the maximum scaling factor $1/S_N(K, j_{\max})$, the rightmost C route in Fig. 2(b) for the global-coupling case is transformed into the C route for the nonglobal-coupling case and the critical scaling behaviors at the critical line segment are also the same as those for the global-coupling case.

5. Summary

In order to confirm the the new critical behaviors found in the abstract system of the coupled 1D maps,[12] we have studied the critical scaling behaviors of synchronous period doublings of the synchronous periodic orbits in a real system of coupled MO's for the case of various couplings. It has been thus found that the structure of the critical set and the critical scaling behaviors are the same as those in the abstract system of the coupled 1D maps. Hence we believe that the critical behaviors in the abstract system of the coupled 1D maps may be observed in a real system consisting of symmetrically coupled identical subsystems.

Acknowledgment

The author would like to thank K. Lee for his assitance in the numerical computations. This work was supported by the Korea Research Foundation under Project No. 1998-015-D00065 and by the Biomedlab Inc.

References

1. R. V. Buskirk and C. Jeffries, *Phys. Rev.* **A31**, 3332 (1985).
2. P. Hadley and M. R. Beasley, *Appl. Phys. Lett.* **50**, 621 (1987); P. Hadley, M. R. Beasley and K. Wiesenfeld, *Phys. Rev.* **B38**, 8712 (1988).
3. S. H. Strogatz, C. M. Marcus, R. M. Westervelt and R. E. Mirollo, *Physica* **D36**, 23 (1989).
4. Y. Kuramoto, *Chemical Oscillations, Waves and Turbulence* (Springer-Verlag, New York, 1984).
5. A. T. Winfree, *The Geometry of Biological Time* (Springer-Verlag, Berlin, 1980).
6. V. Croquette and C. Poitou, *J. Phys. Lett.* **42**, 537 (1981).
7. H. Meissner and G. Schmidt, *Am. J. Phys.* **54**, 800 (1986).
8. K. Briggs, *Am. J. Phys.* **55**, 1083 (1987).
9. S.-Y. Kim (to be published. chao-dyn/9902005).
10. S.-Y. Kim and K. Lee, *Phys. Rev.* **E53**, 1579 (1996).
11. M. J. Feigenbaum, *J. Stat. Phys.* **19**, 25 (1978); *ibid.* **21**, 669 (1979).
12. S.-Y. Kim and H. Kook, *Phys. Rev.* **A46**, R4467 (1992); *Phys. Lett.* **A178**, 258 (1993); *Phys. Rev.* **E48**, 785 (1993); in *the Proceeding of the First International Workshop on Nonlinear Dynamics and Chaos*, ed. H. Lee (Pohang Institute of Science and Technology, Pohang, Korea, 1993), pp. 49–90.
13. I. Waller and R. Kapral, *Phys. Rev.* **A30**, 2047 (1984).
14. V. I. Arnold, *Ordinary Differential Equations* (MIT Press, Cambridge, 1973), p. 114.
15. S.-Y. Kim and B. Hu, *Phys. Rev.* **A44**, 934 (1991); S.-Y. Kim and D.-S. Lee, *ibid.* **A45**, 5480 (1992).
16. J. Guckenheimer and P. Holmes, *Nonlinear Oscillations, Dynamical Systems and Bifurcations of Vector Fields* (Springer-Verlag, New York, 1983), Sec. 3.5.
17. A. J. Lichtenberg and M. A. Lieberman, *Regular and Stochastic Motion* (Springer-Verlag, New York, 1983), Sec. 5.3.
18. S.-Y. Kim, *Phys. Rev.* **E49**, 1745 (1994).
19. J.-M. Mao and B. Hu, *J. Stat. Phys.* **46**, 111 (1987); *Int. J. Mod. Phys.* **B2**, 65 (1988); C. Reick, *Phys. Rev.* **A45**, 777 (1992).

20. Unlike the case of the first period-doubling transition to chaos with only one "stability tree" consisting of connected stability regions of synchronous orbits of all levels, several separate stability trees are found in the $A-c$ plane for the case of the second period-doubling transition to chaos. Only the stability tree starting from the stability region of the stationary point including the $c = 0$ line is shown in Fig. 5, whose structure is essentially the same as that in Fig. 2(a). However, other separate stability trees grow like chimneys without U-shape branchings, as in Fig. 2(b), where the critical scaling behaviors are also the same as those in the C-route for the first period-doubling transition case.